


## Enhancement of mesoscopic fluctuations in transmission of light through a disordered medium at grazing angles

K. A. Kondrat'ev,<sup>1</sup> V. V. Marinyuk ,<sup>1</sup> D. B. Rogozkin,<sup>1,2</sup> and S. V. Sheberstov<sup>3</sup>

<sup>1</sup>*Moscow Engineering Physics Institute (National Research Nuclear University), Kashirskoe Shosse 31, Moscow 115409, Russia*

<sup>2</sup>*N. L. Dukhov All-Russia Research Institute of Automatics, Sushchevskaya Street 22, Moscow 127055, Russia*

<sup>3</sup>*Shirshov Institute of Oceanology, Russian Academy of Sciences, Nahimovskiy prospect 36, Moscow 117997, Russia*



(Received 28 April 2020; revised 6 October 2020; accepted 17 December 2020; published 12 January 2021)

We study how intensity fluctuations in transmission through a disordered slab change depending on the regime of wave transport. A system with large (compared to the wavelength of light) inhomogeneities is considered. Within a diagrammatic approach, the variance of the total transmission coefficient is calculated numerically beyond the diffusion approximation. A great enhancement of fluctuations is found in the crossover from the ballistic to the diffusive transport at the grazing angles of incidence on the sample surface. The effect originates from the reflection of waves that propagate nearly parallel to the sample boundaries and experience scattering through small angles, and reveals itself both in transmission and reflection and in correlations between the transmitted and reflected fluxes.

DOI: [10.1103/PhysRevA.103.013715](https://doi.org/10.1103/PhysRevA.103.013715)

### I. INTRODUCTION

Correlated fluctuations of the intensity of light propagating in a disordered medium are one of the best-known mesoscopic effects [1]. Currently, this effect becomes an important tool for the coherent control of energy transmission [2–5], imaging [5–13], and information transfer [14,15] through highly scattering turbid media.

The intensity correlations are due to the interference of multiply scattered waves and are characterized by different amplitudes and spatial scales [1,5,16]. Short-range correlations (with a spatial scale of the order of the wavelength) have an amplitude of the order of average intensity. The amplitude of long-range correlations is much less, but due to the large spatial scale (greater than the mean free path), they make the main contribution to fluctuations of the total transmission coefficient and the conductance. Relative fluctuations of these quantities do not vanish with increasing the sample size, but grow (i.e., these quantities are non-self-averaging ones [1]).

In disordered media with no absorption, an appearance of fluctuations in the total transmitted flux is due to the wave trajectories reflected from the medium (no reflection means no fluctuations). Therefore, fluctuations of the total transmitted flux can be observed in the case that the reflection of waves is noticeable. Such a situation occurs, for example, in the transmission of waves through the sample of thickness  $L$  greater than the transport mean free path  $l_{tr}$ , i.e., in the diffusive regime of multiple wave scattering. In this regime, the transmitted flux fluctuations are well studied (see, e.g., Refs. [1,5,16] and references therein).

In the transmission of light through relatively thin samples ( $L < l_{tr}$ ) with large inhomogeneities, where highly forward scattering occurs [17] (see also Refs. [10–12]), the situation can be quite different, depending on the incidence angle. If

the direction of incidence does not differ much from the normal one, the total transmission coefficient tends to unity, and its fluctuations turn out to be small. At grazing incidence ( $\pi/2 - \theta_0 \ll 1$ , where  $\theta_0$  is the angle between the direction of light incidence and the inward normal to the input boundary of the sample), the light can be effectively reflected due to small-angle multiple scattering, and one can expect the enhancement of the transmitted flux fluctuations.

A distinctive role of multiple scattering at grazing angles was first noted in Ref. [18] (see also Ref. [19] and references therein) where the albedo problem for a solid state target irradiated by fast charged particles was studied. Further development of the transport theory at grazing angles was given in Refs. [20–22]. The small-angle approximation underlying the results [18–22] is equally applicable to the multiple scattering of light by large (compared to the wavelength) inhomogeneities [23,24]. Scattering at grazing angles can also be important for electron transport through mesoscopic systems [25]. In particular, small-angle scattering of electrons moving nearly parallel to the input and output boundaries is responsible for conductance fluctuations and destruction of conductance quantization in disordered wires [26]. As was shown in Ref. [27], the enhancement of the conductance fluctuations in the crossover from the ballistic to the diffusive regime can also be explained by multiple wave scattering at grazing angles.

In this paper, we study fluctuations in the flux transmitted through a plane slab of a highly forward scattering medium. Our approach is based on the diagrammatic calculations beyond the diffusion approximation. The variance of the total transmission coefficient is expressed in terms of the intensity propagators which are calculated numerically with the transport equation. The single-scattering angular profile is modeled by the Henyey-Greenstein function (see, e.g., Refs. [16,17]).

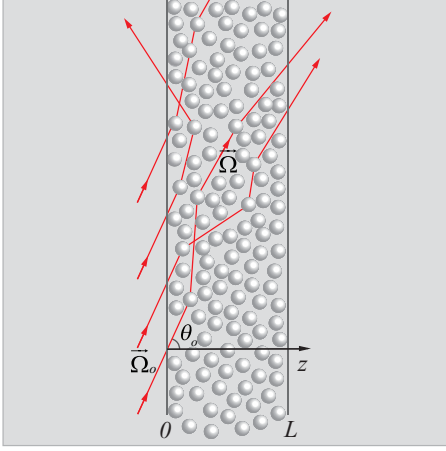


FIG. 1. Scattering geometry.

We show that the fluctuations are enhanced with increasing the angle of incidence  $\theta_0$ . A great, up to a hundred times, enhancement of the fluctuations is attained in the crossover from the ballistic to the diffusive regime at grazing angles,  $\pi/2 - \theta_0 \ll 1$ , where the transport of waves occurs nearly parallel to the sample boundaries. In the  $L$  dependence of the variance of relative transmission fluctuations, a local peak appears at  $L \sim l\vartheta_0$ , where  $l$  is the mean free path and  $\vartheta_0$  is the characteristic angle of single scattering. As the sample thickness  $L$  increases from  $l\vartheta_0$  to  $l_{tr}$ , the relative transmission fluctuations remain to be nearly  $L$  independent. The behavior of the variance at subdiffusive scales ( $L < l_{tr}$ ) is shown to be governed by the competition between the contributions of short- and long-range correlations.

## II. BASIC RELATIONS

Consider a plane wave incident upon a sample of a disordered medium in direction  $\mathbf{\Omega}_0$  (see Fig. 1). Under conditions of weak localization ( $\lambda \ll l$ , where  $\lambda$  is the wavelength), the total transmission coefficient  $\langle T \rangle$  averaged over disorder is governed by the sum of ladder diagrams [1,16] and can be expressed in terms of the intensity propagator,

$$\langle T \rangle = \int_{\mu>0} \mu I(z=L, \mathbf{\Omega}|z_0=0, \mathbf{\Omega}_0) d\mathbf{\Omega}, \quad (1)$$

where  $\mu = \Omega_z$ , the  $z$  axis is directed along the inward normal to the input boundary of the sample, and  $L$  is the sample thickness. The propagator  $I(z, \mathbf{\Omega}|z_0, \mathbf{\Omega}_0)$  denotes the average intensity at depth  $z$  in direction  $\mathbf{\Omega}$  from a source placed at depth  $z_0$  and emitting waves in direction  $\mathbf{\Omega}_0$ . The intensity  $I$  is subject to the transport equation [17]

$$\begin{aligned} \mu \frac{\partial}{\partial z} I(z, \mathbf{\Omega}|z_0, \mathbf{\Omega}_0) &= \delta(z-z_0) \delta(\mathbf{\Omega} - \mathbf{\Omega}_0) \\ &+ n \int d\mathbf{\Omega}' \frac{d\sigma}{d\Omega}(\mathbf{\Omega}\mathbf{\Omega}') [I(z, \mathbf{\Omega}'|z_0, \mathbf{\Omega}_0) \\ &- I(z, \mathbf{\Omega}|z_0, \mathbf{\Omega}_0)], \end{aligned} \quad (2)$$

where  $n$  is the number of scattering centers per unit volume, and  $d\sigma/d\Omega$  is the differential cross section of elastic scattering. It is assumed that there is no absorption in the medium.

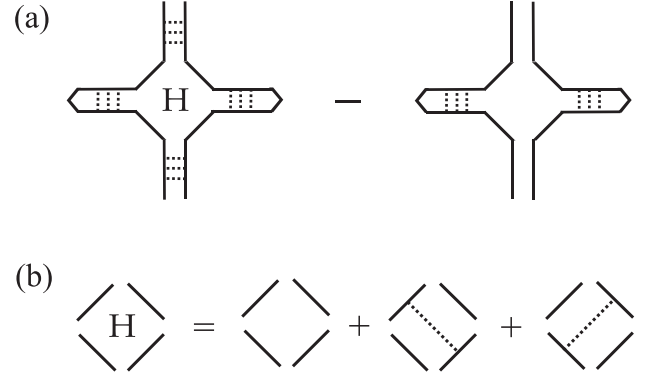


FIG. 2. (a) Feynman diagrams for calculating the variance of the transmission coefficient. Converging solid lines to a point denotes summation over all outgoing modes. Ladder graphs correspond to the intensity propagators. (b) Diagrams for the Hikami vertex [28]. Solid lines denote the average Green's function or its complex conjugate. Dashed lines connect identical scatterers.

The variance of the total transmission coefficient  $\langle (\delta T)^2 \rangle$  can be represented as an expansion in orders of interference between ladders. Each interference event between the ladders contains the Hikami vertex [28]. The principal contribution to  $\langle (\delta T)^2 \rangle$  (i.e., the leading term of expansion in  $\lambda/l$ ) is governed by the single-Hikami-vertex diagram [29,30] (see Fig. 2 and Refs. [1,16,31] for review). In the ladders appearing in Fig. 2(a), we take into account all orders of wave scattering events, including wave propagation without any scattering. Contrary to calculations when performed within the diffusion approximation, we need not introduce a separate diagram for the contribution from short-range (or the so-called  $C_1$  [1,16]) correlations. Such a diagram is already contained in Fig. 2. It corresponds to the empty Hikami vertex and outgoing lines with no scattering.

A straightforward calculation of the diagram shown in Fig. 2 can be performed beyond the diffusion approximation (see Appendix A and Refs. [32–34]). The expression for the variance has the form

$$\begin{aligned} \langle (\delta T)^2 \rangle &= \frac{\pi}{N} n \int_0^L dz \iint d\mathbf{\Omega} d\mathbf{\Omega}' \frac{d\sigma}{d\Omega}(\mathbf{\Omega}\mathbf{\Omega}') \\ &\times [I_f(L|z, \mathbf{\Omega}) - I_f(L|z, \mathbf{\Omega}')]^2 I_i(z, \mathbf{\Omega}) I_i(z, \mathbf{\Omega}'), \end{aligned} \quad (3)$$

where  $N = k_0^2 A / 4\pi$  is the number of propagating modes,  $k_0 = 2\pi/\lambda$  is the wave number, and  $A$  is the area of the sample surface. The incoming propagator  $I_i(z, \mathbf{\Omega})$  denotes the intensity at depth  $z$  in direction  $\mathbf{\Omega}$ , for a plane wave incident upon the slab boundary at  $z=0$  in direction  $\mathbf{\Omega}_0$ ,

$$I_i(z, \mathbf{\Omega}) = I(z, \mathbf{\Omega}|z=0, \mathbf{\Omega}_0). \quad (4)$$

The outgoing propagator,

$$I_f(L|z, \mathbf{\Omega}) = \int_{\mu'>0} d\mathbf{\Omega}' \mu' I(z=L, \mathbf{\Omega}'|z, \mathbf{\Omega}), \quad (5)$$

is the total flux outgoing through the boundary at  $z=L$  from a plane source placed at depth  $z$  and emitting waves in direction  $\mathbf{\Omega}$ . Due to integrating over  $\mathbf{\Omega}'$ , the propagator  $I_f$  depends only

on  $\mu = \Omega_z$ . The values  $\langle T \rangle$  and  $\langle (\delta T)^2 \rangle$  are normalized to the unit  $z$  component of the incident flux.

Equation (3) can also be derived with the results of Refs. [35,36] obtained within the Boltzmann-Langevin approach. Equation (3) establishes the interrelation between the variance of transmission coefficient fluctuations and the characteristics of the scattering sample. In the limit  $\lambda \ll l$ , Eq. (3) is the exact result in the sense that it is applicable both for an arbitrary angular dependence of the differential cross section and for an arbitrary regime of wave propagation (from the ballistic regime to the diffusive one).

Expressions analogous to Eq. (3) can also be derived both for the variance of the reflection coefficient  $\langle (\delta R)^2 \rangle$  and for the covariance between the transmission and reflection coefficients  $\langle \delta T \delta R \rangle$ . For  $\langle (\delta R)^2 \rangle$ , the corresponding expression is obtained from Eq. (3) by changing the definition of the outgoing propagator. The intensity  $I(z=0, \Omega'|z, \Omega)$  should be substituted for  $I(z=L, \Omega'|z, \Omega)$  to Eq. (5). For the covariance  $\langle \delta T \delta R \rangle$ , the factor  $[I_f(L|z, \Omega) - I_f(L|z, \Omega')]^2$  should be replaced by  $[I_f(L|z, \Omega) - I_f(L|z, \Omega')][I_f(0|z, \Omega) - I_f(0|z, \Omega')]$ . In the case of a medium with no absorption, the flux conservation,  $T + R = 1$ , gives  $\delta T + \delta R = 0$ , and, as a result, both these quantities are expressed in terms of the variance of the transmission coefficient,

$$\langle (\delta R)^2 \rangle = -\langle \delta T \delta R \rangle = \langle (\delta T)^2 \rangle.$$

If the thickness of the sample exceeds the transport mean free path,  $L \gg l_{tr}$ , the propagators depend only slightly on the angular variables and can be expanded in a series of the Legendre polynomials [37]. In this case, Eq. (3) transforms [33,34] to the well-known result of the diffusion theory,

$$\langle (\delta T)^2 \rangle = \frac{L}{2Nl_{tr}} \langle T \rangle^2. \quad (6)$$

Equation (6) can be rewritten in terms of the dimensionless conductance  $\langle g \rangle = 4Nl_{tr}/3L$  as  $\langle (\delta T)^2 \rangle / \langle T \rangle^2 = 2/3 \langle g \rangle$  [1,16]. In the diffusive regime, the average transmission coefficient  $\langle T \rangle$  is proportional to the ratio  $l_{tr}/L$ , and the variance  $\langle (\delta T)^2 \rangle$  falls off inversely proportional to the sample thickness  $L$ . Relative fluctuations, on the contrary, increase linearly with increasing  $L$ ,  $\langle (\delta T)^2 \rangle / \langle T \rangle^2 \sim L$ . Equation (6) determines a leading term in the expansion of the variance  $\langle (\delta T)^2 \rangle$  in powers of  $l_{tr}/L$ . As follows from the results of our numerical calculations performed with Eq. (3) for a highly forward scattering medium (see Fig. 3), a deviation from the diffusion formula (6) grows noticeably as the angle of incidence increases.

### III. FLUCTUATIONS IN A HIGHLY FORWARD SCATTERING MEDIUM

Up to now, the transmission fluctuations were studied for the diffusive regime ( $L > l_{tr}$ ), in which the ratio  $l_{tr}/L$  is the only parameter affecting the wave transport in the medium. As shown below, a novel effect arises in the wave transmission through samples of subdiffusive thickness ( $L < l_{tr}$ ) and particularly in the case of highly forward single scattering,  $l/l_{tr} = 1 - g \ll 1$ , where  $g$  is the mean cosine of the single-scattering angle (the so-called asymmetry factor) [17,37].

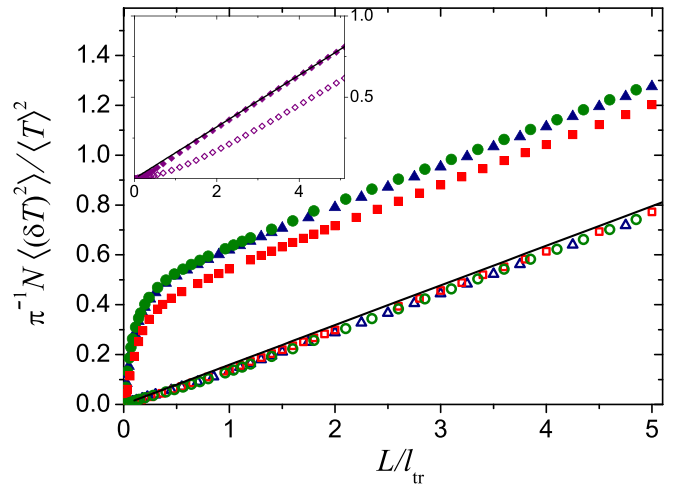


FIG. 3. Relative fluctuations of the total transmission coefficient as a function of transport optical thickness  $L/l_{tr}$ . Symbols are the results of numerical calculations with Eqs. (1)–(3) by the discrete-ordinate method. The solid line is the diffusion formula (6). The results for normal ( $\theta_0 = 0$ ) and oblique ( $\theta_0 = 60^\circ$ ) incidence are shown by open and solid symbols, respectively. The mean cosine of the single-scattering angle equals  $g = 0.9$  (squares),  $g = 0.95$  (triangles), and  $g = 0.96$  (circles). The inset illustrates the change in relative transmission fluctuations for  $g = 0$ .

To model single scattering in the medium we take advantage of the Henyey-Greenstein differential cross section,

$$\frac{d\sigma}{d\Omega}(\cos \vartheta) = \frac{\sigma}{4\pi} \frac{1 - g^2}{(1 + g^2 - 2g \cos \vartheta)^{3/2}}, \quad (7)$$

where  $\sigma$  is the elastic cross section. The mean free path  $l$  is related to  $\sigma$  by  $l = (n\sigma)^{-1}$ . Equation (7) is used very widely to simulate highly forward scattering of light in random media with large inhomogeneities [16,17,37,38].

To study the dependence of the variance  $\langle (\delta T)^2 \rangle$  on the sample parameters, we perform the numerical integration of Eq. (3). The intensity propagators entering into Eq. (3) are calculated from the transport equation (2) with a numerical code based on the discrete-ordinate method [17,37] (regarding application to highly forward scattering, see, e.g., Refs. [39,40]). It is assumed that coherent reflection of light from the sample boundaries can be neglected (e.g., the sample presents a layer of particles embedded in a uniform medium, or the disordered sample is placed in a medium with the refractive index equal to that of the sample—see Refs. [41–43] on refractive-index matching). The corresponding restrictions are discussed in Appendix B.

The results of our calculations are presented in Figs. 3–6. The dependence of relative fluctuations  $\langle (\delta T)^2 \rangle / \langle T \rangle^2$  on the sample thickness  $L$  is illustrated in Fig. 3 for both normal and oblique incidence. In the diffusive limit, the results of our numerical calculations are approximated by the relation

$$\frac{\langle (\delta T)^2 \rangle}{\langle T \rangle^2} = \frac{1}{2N} \left( \frac{L}{l_{tr}} + \Delta \right). \quad (8)$$

The first term in Eq. (8) is coincident with the diffusion formula (6). The second one that is responsible for the deviation from the diffusion result depends both on the angle of

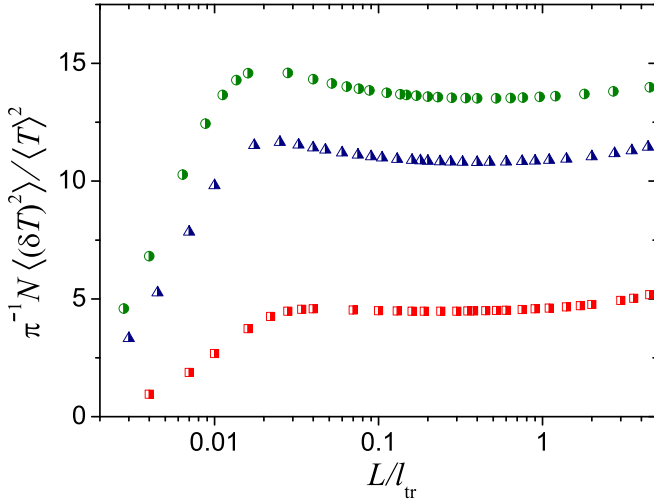


FIG. 4. Thickness dependence of the relative fluctuations of the total transmission coefficient at grazing incidence,  $\mu_0 = 0.1$ . From lower to upper graphs,  $g = 0.9, 0.95$ , and  $0.96$ .

incidence  $\theta_0$  and on the asymmetry factor  $g$  of single scattering,  $\Delta = \Delta(\theta_0, g)$ . For isotropic scattering ( $g = 0$ ), the value of  $\Delta$  is negative and remains small at oblique incidence (see the inset in Fig. 3). Contrary, for highly forward scattering ( $1 - g \ll 1$ ),  $\Delta$  increases noticeably with increasing  $\theta_0$  and far exceeds unity,  $\Delta \gg 1$ , in the limit of grazing angles of incidence,  $\pi/2 - \theta_0 \ll 1$ . Moreover, in this case, the  $L$  dependence of  $\langle (\delta T)^2 \rangle / \langle T \rangle^2$  becomes nonmonotonous (see Fig. 4). There appear a local maximum at  $L \sim l(1 - g)$  and a plateau in the range  $l(1 - g) < L < l_{tr} = l/(1 - g)$ . The plateau is expanded as the asymmetry factor  $g$  tends to unity.

The enhancement of  $\langle (\delta T)^2 \rangle / \langle T \rangle^2$  at grazing incidence is not only due to a decrease in the transmission coefficient  $\langle T \rangle$ . The main reason is that the variance of transmission fluctuations  $\langle (\delta T)^2 \rangle$  grows drastically with decreasing  $\mu_0 = \cos \theta_0$  in the case of highly forward scattering,  $1 - g \ll 1$  [see Fig. 5—the peak value of  $\langle (\delta T)^2 \rangle$  increases a hundred times as  $\mu_0$  decreases from 1 to 0.1]. For  $g = 0$ , the tendency is opposite: the peak value of the variance  $\langle (\delta T)^2 \rangle$  decreases with increasing the angle  $\theta_0$ . This is illustrated in Fig. 6 where the results of numerical calculations with Eq. (3) for  $g = 0$  and  $g = 0.9$  are compared.

A dramatic enhancement of the fluctuations is observable for samples of subdiffusive thickness,  $L < l_{tr}$ . In this case, multiple wave scattering occurs predominantly through small angles, and, therefore, only the waves incoming nearly parallel to the boundary of the sample can be effectively reflected from it. These are precisely the waves that are responsible for fluctuations of the total transmission coefficient (if there is no reflection, the coefficient  $T$  equals unity and does not fluctuate).

A distinctive role of the wave trajectories that are nearly parallel to the input and output boundaries of the sample can also be understood from an analysis of the angular dependence of the factor

$$\frac{1}{\sigma} \frac{d\sigma}{d\Omega}(\mathbf{\Omega}\mathbf{\Omega}') [I_f(L|z, \mu) - I_f(L|z, \mu')]^2 \quad (9)$$

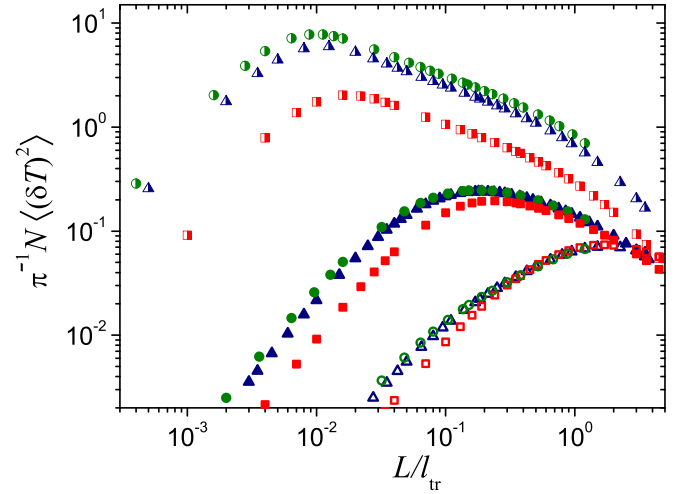


FIG. 5. Variance of fluctuations of the total transmission coefficient as a function of the transport optical thickness  $L/l_{tr}$ . Symbols are the results of numerical calculations with Eq. (3). Open, solid, and half-solid symbols correspond to  $\mu_0 = 1, \mu_0 = 0.5$ , and  $\mu_0 = 0.1$ , respectively. The mean cosine of the single-scattering angle equals  $g = 0.9$  (squares),  $g = 0.95$  (triangles), and  $g = 0.96$  (circles).

entering into the general expression (3). This factor is independent of the characteristics of the incident light and is governed only by the parameters of the scattering sample (its thickness, the single-scattering law, etc.). The quantity (9) is responsible for the transfer of the bulk speckle to the output boundary of the sample. The speckle is formed by interference of the waves propagating in different directions  $\mathbf{\Omega}$  and  $\mathbf{\Omega}'$ . The difference between the outgoing propagators appearing in Eq. (9) describes the difference in the probabilities that the waves propagating in the directions  $\mathbf{\Omega}$  and  $\mathbf{\Omega}'$  reach the output boundary. Fluctuations of the total transmission coefficient arise provided that the probability to reach the output

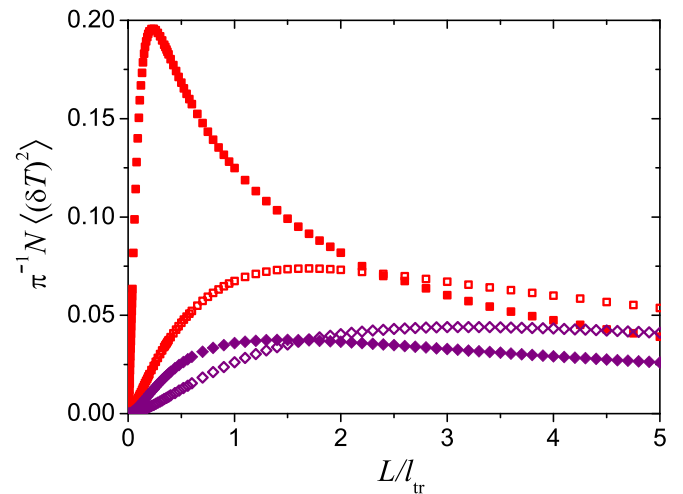


FIG. 6. Thickness dependence of transmission fluctuations at different angles of incidence. Open and solid symbols correspond to  $\mu_0 = 1$  and  $\mu_0 = 0.5$ , respectively. The mean cosine of the single-scattering angle equals  $g = 0$  (diamonds) and  $g = 0.9$  (squares).

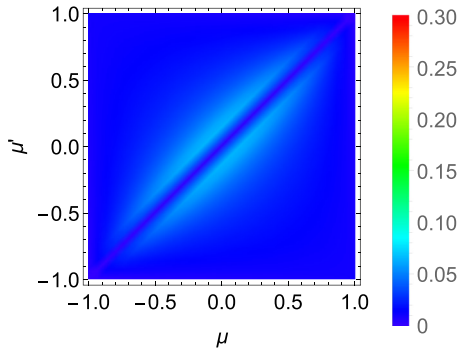


FIG. 7. Angular dependence of the factor (9) in the diffusive regime. The azimuthal angles of directions  $\Omega$  and  $\Omega'$  are equal to each other. The mean cosine of the single-scattering angle is  $g = 0.9$ , and the transport optical thickness of the sample is  $L/l_{tr} = 5$ . The outgoing propagators are calculated within the diffusion approximation.

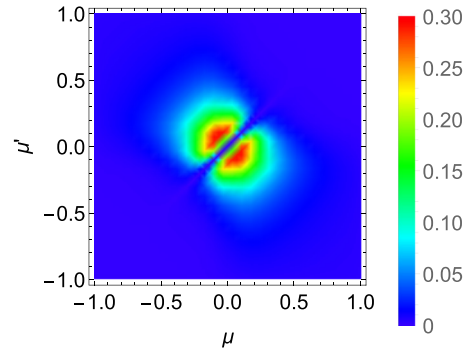


FIG. 8. Angular dependence of the factor (9) in the subdiffusive case. The azimuthal angles of directions  $\Omega$  and  $\Omega'$  are equal to each other. The mean cosine of the single-scattering angle is  $g = 0.9$ , the transport optical thickness of the sample is  $L/l_{tr} = 0.05$ ,  $z = L/2$ . The outgoing propagators are calculated numerically with the discrete-ordinate method.

boundary is different depending on the direction of wave propagation. Otherwise, the total transmission coefficient does not fluctuate.

Correlation in fluctuations is due to the passing of waves through the same scatterer. As the single-scattering cross section (7) entering into Eq. (9) falls off rapidly with increasing the angle  $\vartheta = \arccos \Omega \Omega'$ , the directions  $\Omega$  and  $\Omega'$  can differ by no more than the characteristic single-scattering angle  $\vartheta_0 = 1 - g$ . As for the difference between the propagators  $[I_f(L|z, \mu) - I_f(L|z, \mu')]$ , it is governed by the regime of multiple scattering of waves.

In the diffusive regime,  $L \gg l_{tr}$ , expansion of the propagators in terms of the Legendre polynomials gives

$$I_f(L|z, \mu) - I_f(L|z, \mu') = \frac{3}{4\pi}(\mu - \mu')J_f(z),$$

where  $J_f(z) = \int \mu I_f(L|z, \mu) d\Omega$ . In the considered case of the medium with no absorption,  $J_f$  is  $z$  independent,  $J_f = 4\pi l_{tr}/3L$ . The angular dependence of the factor (9) in the diffusive regime is illustrated in Fig. 7. As follows from the figure, the factor (9) selects pairs of trajectories in two close directions. These directions can be oriented arbitrarily with respect to the sample boundaries.

For a sample of subdiffusive thickness,  $L < l_{tr}$ , where the small-angle regime of multiple scattering is realized, the outgoing propagator  $I_f(L|z, \mu)$  proves to be a steplike function of the angular variable  $\mu$ . For waves propagating toward the output boundary ( $\mu > 0$ ), the outgoing propagator is close to unity,  $I_f(L|z, \mu) \approx 1$ , otherwise ( $\mu < 0$ ),  $I_f(L|z, \mu) \ll 1$ . The blurring of the step function in the vicinity of  $\mu = 0$  is due to the possibility of the reflection of waves propagating at grazing angles (i.e., in directions that are nearly parallel to the input and output boundaries). Taking into account the highly elongated angular dependence of the single-scattering cross section ( $1 - g \ll 1$ ), we find that the factor (9) differs from zero only for directions  $|\mu|, |\mu'| \ll 1$ . This is confirmed by the result of our numerical calculations shown in Fig. 8. Thus, for  $L < l_{tr}$ , the quantity (9) acts as a modulating factor which selects trajectories that are nearly parallel to the medium surface.

The above reasoning is concerned with the significance of grazing paths for wave transport through thin samples,  $L < l_{tr}$ . As for the enhancement of transmission fluctuations, this effect is due to increasing the average intensity at grazing angles of wave propagation. The matter is that a source of the fluctuations of the total transmission (or reflection) coefficient is the bulk speckle arising due to wave interference inside of the sample [1,16]. The amplitude of intensity fluctuations in the bulk speckle is proportional to the average intensity, which increases greatly at grazing angles (see, e.g., Refs. [37,44]). This can be illustrated most clearly by the single-scattering intensity,

$$I_i(z, \Omega) = \frac{1}{\mu\mu_0} \frac{1}{\sigma} \frac{d\sigma}{d\Omega} (\Omega \Omega_0) \frac{z}{l},$$

which grows in the case of highly forward scattering at grazing angles, because  $\mu, \mu_0 \ll 1$  and  $(1/\sigma)d\sigma/d\Omega \gg 1$  simultaneously. For thin samples,  $L < l_{tr}$ , the portion of radiation propagating at grazing angles ( $\mu, \mu_0 \ll 1$ ) proves to be principal and, therefore, the amplitude of fluctuations in the bulk speckle increases. As the thickness of the sample becomes larger,  $L > l_{tr}$ , the spread of waves over directions at grazing angles decreases. As a result, the amplitude of fluctuations in the bulk speckle is lowered, and the value of  $\langle (\delta T)^2 \rangle$  decreases with increasing the sample thickness.

The enhancement of fluctuations at grazing angles is also reflected on the  $L$  dependence of the relative covariance between the transmission and reflection coefficients,  $\langle \delta T \delta R \rangle / \langle T \rangle \langle R \rangle$ . Note that negative transmission-reflection correlations are of importance for imaging through scattering media and currently being actively studied [3,9,13–15]. Our results as applied to the relative covariance are illustrated in Fig. 9. As follows from the figure, the  $L$  dependence of the covariance  $\langle \delta T \delta R \rangle / \langle T \rangle \langle R \rangle$  has a minimum at subdiffusive scales,  $L < l_{tr}$ . As the angle of incidence  $\theta_0$  increases, the minimum is deepened and shifted to the region of lesser  $L$ . For a given sample thickness, the correlations between the transmitted and reflected fluxes are enhanced with increasing the angle  $\theta_0$  and the mean cosine  $g$ .

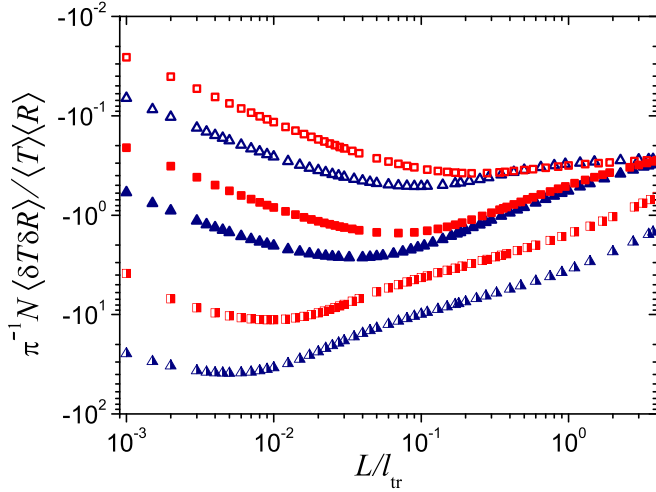


FIG. 9. Relative covariance between the transmission and reflection coefficients as a function of the transport optical thickness  $L/l_{tr}$ . Open, solid, and half-solid symbols correspond to  $\mu_0 = 1$ ,  $\mu_0 = 0.5$ , and  $\mu_0 = 0.1$ , respectively. The mean cosine of the single-scattering angle equals  $g = 0.9$  (squares) and  $g = 0.95$  (triangles).

#### IV. WAVE TRANSPORT AT GRAZING INCIDENCE

If the thickness of the medium is less than the transport mean free path,  $L < l_{tr}$ , isotropization of waves over directions does not occur and the diffusive regime of wave propagation does not develop. In this case, multiple scattering has a small-angle character, and the variance of fluctuations depends significantly on the angle of incidence. For the incidence close to normal ( $\mu_0 = \cos \theta_0 \approx 1$ ), almost all of the incident light is transmitted through the medium,  $\langle T \rangle \approx 1$ , and the fluctuations prove to be small (see Fig. 3). As the angle of incidence  $\theta_0$  increases, the reflection of light and, as a consequence, the fluctuations of the transmission coefficient increase too. A considerable enhancement of fluctuations should be expected at grazing angles of incidence,  $\pi/2 - \theta_0 \ll 1$ , where the incident light can be effectively reflected from the medium due to small-angle multiple scattering.

The radiative transfer theory at grazing incidence was elaborated in Refs. [18–24] on the basis of the small-angle approximation. In this case, we can simplify the general equations (1)–(3) using the relations [18–24]

$$\mu = \cos \theta = \sin \zeta \approx \zeta, \quad (10)$$

$$2(1 - \mathbf{\Omega} \mathbf{\Omega}') \approx (\zeta - \zeta')^2 + (\varphi - \varphi')^2, \quad (11)$$

where  $\zeta = \pi/2 - \theta$  is the angle between the direction  $\mathbf{\Omega}$  and the medium boundary, and  $\varphi$  is the azimuth angle of the direction  $\mathbf{\Omega}$ . As is customary in the small-angle approximation (see, e.g., Ref. [17]), the angles  $\zeta$  and  $\varphi$  are thought of as varying within infinite limits,

$$\int d\mathbf{\Omega} \dots = \int_{-\infty}^{\infty} d\zeta \int_{-\infty}^{\infty} d\varphi \dots \quad (12)$$

The intensity propagator  $I(z, \mathbf{\Omega}|z_0, \mathbf{\Omega}_0) \equiv I(z, \zeta, \varphi|z_0, \zeta_0, \varphi_0)$  is assumed to decrease rapidly as the values of  $|\zeta|$  and  $|\varphi|$  increase. In the considered approximation, Eq. (3) takes the

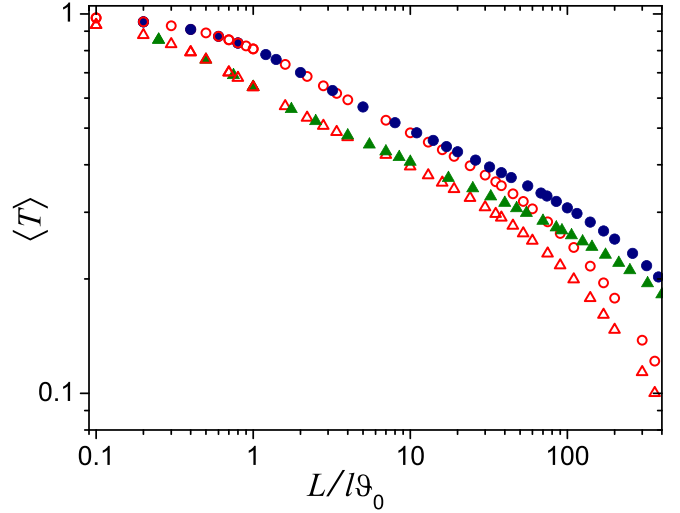


FIG. 10. Average total transmission coefficient in dimensionless variables. Symbols are the results of numerical calculations with Eq. (1). Open and solid symbols correspond to  $\zeta_0 = \vartheta_0/2 = 0.05$  and  $\zeta_0 = \vartheta_0/2 = 0.02$ , respectively (two upper graphs), and to  $\zeta_0 = \vartheta_0 = 0.1$  and  $\zeta_0 = \vartheta_0 = 0.05$ , respectively (two lower graphs).

form

$$\begin{aligned} \langle (\delta T)^2 \rangle &= \frac{\vartheta_0}{2Nl} \int_0^L dz \iiint \int_{-\infty}^{\infty} d\zeta d\varphi d\zeta' d\varphi' \\ &\times \frac{[I_f(z, \zeta') - I_f(z, \zeta)]^2 I_i(z, \zeta, \varphi) I_i(z, \zeta', \varphi')}{[\vartheta_0^2 + (\zeta - \zeta')^2 + (\varphi - \varphi')^2]^{3/2}}, \end{aligned} \quad (13)$$

where  $\vartheta_0 = 1 - g \ll 1$  is the characteristic angle of single scattering, and  $l$  is the mean free path.

Within the small-angle approximation, the solution to the transport equation (2) is expressed in terms of a function of dimensionless variables,

$$I(z, \zeta, \varphi|z_0, \zeta_0, \varphi_0) = \frac{1}{\vartheta_0^3} f\left(\frac{z}{L}, \frac{\zeta}{\vartheta_0}, \frac{\varphi - \varphi_0}{\vartheta_0}, \frac{z_0}{L}, \frac{\zeta_0}{\vartheta_0}, \frac{L}{l\vartheta_0}\right). \quad (14)$$

The fact that the intensity propagator can be presented in the form of Eq. (14) enables us to draw a conclusion regarding the  $L$  dependence of the variance of transmission fluctuations  $\langle (\delta T)^2 \rangle$ . Substituting Eq. (14) into Eq. (13), we arrive at the following scaling relation,

$$\langle (\delta T)^2 \rangle = \frac{1}{N\vartheta_0^3} F\left(\frac{L}{l\vartheta_0}, \frac{\zeta_0}{\vartheta_0}\right). \quad (15)$$

A similar relation is also valid for the average transmission coefficient [40],  $\langle T \rangle = \Phi(L/l\vartheta_0, \zeta_0/\vartheta_0)$ .

The validity of the scaling relations for the average transmission coefficient and the variance of fluctuations is illustrated in Figs. 10–12 where our results of numerical integration of Eqs. (1)–(3) with the discrete-ordinate method are presented. Figure 11, for example, illustrates the fact that, for given  $\zeta_0/\vartheta_0$ , the value  $N\vartheta_0^3 \langle (\delta T)^2 \rangle$  is virtually a universal function of  $L/l\vartheta_0$  up to  $L \sim 100l\vartheta_0 \sim l_{tr}$ .

At grazing angles of incidence, three regions can be clearly distinguished in the  $L$  dependence of the variance  $\langle (\delta T)^2 \rangle$ . In

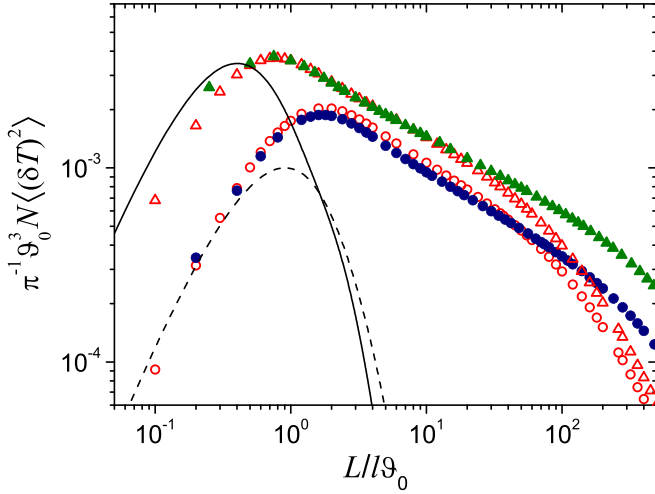


FIG. 11. Variance of the total transmission coefficient in dimensionless variables. Symbols are the results of numerical calculations with Eq. (3). Open and solid symbols correspond to  $\zeta_0 = \vartheta_0/2 = 0.05$  and  $\zeta_0 = \vartheta_0/2 = 0.02$ , respectively (two upper graphs), and to  $\zeta_0 = \vartheta_0 = 0.1$  and  $\zeta_0 = \vartheta_0 = 0.05$ , respectively (two lower graphs). The solid and the dashed curves are the results of calculations within the second-order approximation.

a very thin sample,  $L < l\vartheta_0$ , the variance grows rapidly with increasing  $L$ . In this case, the variance can be calculated by expanding the propagators entering into Eq. (3) in orders of wave scattering. The single-scattering contributions to  $\langle (\delta T)^2 \rangle$  cancel each other (see, e.g., Ref. [33]). The first nonvanishing contribution to  $\langle (\delta T)^2 \rangle$  is governed by the second-order scattering which well describes the rapid growth of fluctuations with increasing  $L$  (see Fig. 11).

The variance reaches its maximum at  $L \sim l\vartheta_0$ , and then, in a rather wide range  $l\vartheta_0 < L < l_{tr}$ , decreases slowly according to a power law  $\sim L^{-\nu}$  with exponent  $\nu \approx 1/3$ . Surprisingly, the  $L$  dependencies of the variance  $\langle (\delta T)^2 \rangle$  and the square of the average coefficient  $\langle T \rangle^2$  are almost identical in this range of thickness. Relative fluctuations of the transmission coefficient prove to be virtually  $L$  independent. This is confirmed by a horizontal “plateau” which is clearly distinguishable in the dependence of the ratio  $\langle (\delta T)^2 \rangle / \langle T \rangle^2$  on the sample thickness (see Figs. 4 and 12).

The plateau in the  $L$  dependence of  $\langle (\delta T)^2 \rangle / \langle T \rangle^2$  is governed by the combined effect of the contributions from long- and short-range intensity correlations to the variance of the transmission coefficient. The contribution from the short-range intensity correlations  $\langle (\delta T)^2 \rangle^{\text{short}}$  is described by that part of the diagram shown in Fig. 2 which contains the empty Hikami box and the outgoing propagators without scattering events (see, e.g., Ref. [33]). The spatial scale of short-range correlations is proportional to the ratio of the wavelength to the characteristic multiple-scattering angle. The contribution  $\langle (\delta T)^2 \rangle^{\text{short}}$  is determined by the expression [33,34]

$$\langle (\delta T)^2 \rangle^{\text{short}} = \frac{\pi}{N} \int_{\Omega_z > 0} d\Omega \Omega_z [I^2(L, \Omega | 0, \Omega_0)]^{\geq 2}, \quad (16)$$

where the superscript ( $\geq 2$ ) indicates that the total number of scattering events in the product of intensity propagators

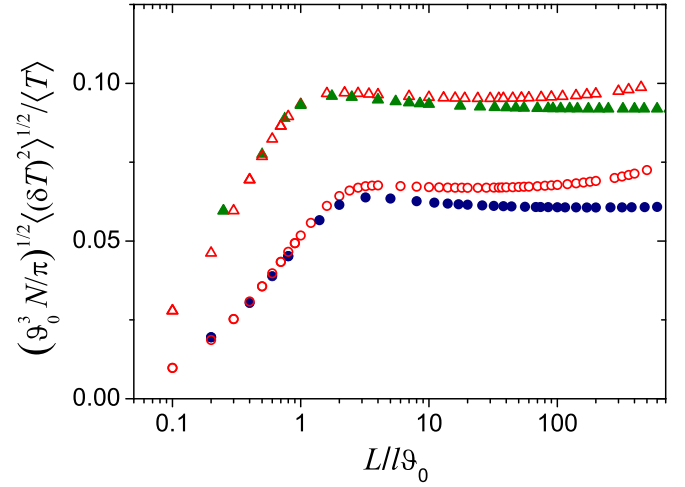


FIG. 12. Relative fluctuations of the total transmission coefficient in dimensionless variables. All symbols correspond to the same parameters as in Figs. 7 and 8.

is greater than or equal to two. The contributions  $\langle (\delta T)^2 \rangle^{\text{short}}$  and  $\langle (\delta T)^2 \rangle^{\text{long}} = \langle (\delta T)^2 \rangle - \langle (\delta T)^2 \rangle^{\text{short}}$  are shown in Fig. 13. From the figure it follows that the contribution from long-range correlations changes its sign at  $l\vartheta_0 < L < l$ . With a further increase in  $L$ , the contribution  $\langle (\delta T)^2 \rangle^{\text{long}}$  becomes dominant. For  $L < l$ , both contributions are equally important. For those values of the sample thickness, where  $\langle (\delta T)^2 \rangle^{\text{long}} < 0$ , intensity fluctuations at large (as compared to the wavelength) distances are negatively correlated. The relationship between the contributions from short- and long-range intensity correlations to the variance  $\langle (\delta T)^2 \rangle$  at  $L < l$  resembles that between the corresponding contributions to the variance of total reflection  $\langle (\delta R)^2 \rangle$  in the diffusive regime (see, e.g., Refs. [14,33,45,46]).

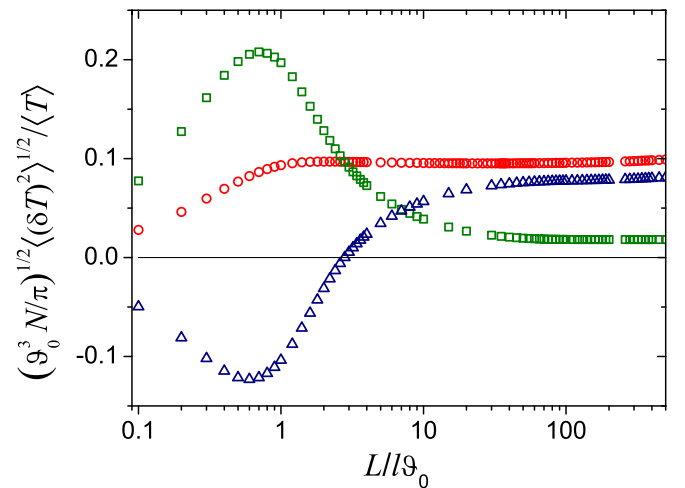


FIG. 13. Different contributions to relative fluctuations of the total transmission coefficient. The contributions from short- and long-range correlations and their sum are shown by squares, triangles, and circles, respectively. The calculations were performed for  $\zeta_0 = 0.05$ ,  $\vartheta_0 = 0.1$ .

As follows from our numerical calculations, the self-similarity law (15) fails as the sample thickness  $L$  becomes larger than  $l_{tr}$ . In this case, the small-angle approximation is no longer valid, and the crossover to the diffusive transport occurs.

Thus, in the case of grazing incidence, the three regimes of wave propagation (low-order scattering, small-angle multiple scattering, and diffusive transport) manifest themselves clearly in the dependence of transmission fluctuations on the sample thickness. The corresponding features are also observable in the relative covariance between the transmitted and reflected fluxes.

### V. CONCLUSIONS

We have presented the results of a detailed analysis of transmitted flux fluctuations in a disordered medium with highly forward scattering. The variance of the total transmission coefficient has been calculated numerically using the discrete-ordinate method. We have shown that, contrary to a medium with isotropically scattering centers, in the highly forward scattering medium the total transmission fluctuations are enhanced dramatically at the grazing incidence of light on the sample surface. This effect reveals itself in the subdiffusive case,  $L < l_{tr}$ , where the sample thickness is less than the transport mean free path and multiple scattering of light occurs through small angles. Our numerical results are in good agreement with the scaling relations derived within the small-angle approximation.

The results obtained give insight into the impact of the regime of wave propagation on the mesoscopic intensity fluctuations and can be applied for studying how the specific features of disorder (e.g., large-scale correlations between inhomogeneities) reveal themselves in phase-coherent transport through complex media.

### APPENDIX A: HIKAMI VERTEX FOR NONPOINT SCATTERERS

In a medium with discrete scatterers, a scalar monochromatic field  $\psi(\mathbf{r})$  obeys the equation

$$[\nabla^2 + k_0^2(1 + \delta\varepsilon(\mathbf{r}))]\psi(\mathbf{r}) = 0, \quad (A1)$$

where  $k_0 = \omega/c$ , and the random part  $\delta\varepsilon$  of dielectric constant has the form

$$\delta\varepsilon(\mathbf{r}) = \sum_a \varepsilon(|\mathbf{r} - \mathbf{r}_a|), \quad (A2)$$

and the vector  $\mathbf{r}_a$  denotes the “a”th scatterer position. The  $z$  component of the density of flux transmitted through the medium is defined as

$$J_z(\boldsymbol{\rho}) = \frac{i}{2k_0} \left( \frac{\partial}{\partial z} - \frac{\partial}{\partial z'} \right) \psi(z', \boldsymbol{\rho}) \psi^*(z, \boldsymbol{\rho}) \Big|_{z'=z=L}, \quad (A3)$$

where the vector  $\boldsymbol{\rho}$  lies in the plane ( $xy$ ) parallel to the slab boundaries. The average transmission coefficient  $\langle T \rangle = \langle J_z \rangle$  can be expressed in terms of the ensemble-average second moment  $\langle \psi \psi^* \rangle$  which is governed by the sum of ladder diagrams [1]. The variance of the total transmission coefficient

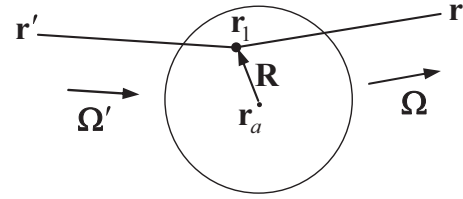


FIG. 14. Diagram element containing one scattering event.

$\langle (\delta T)^2 \rangle$  is given by

$$\langle (\delta T)^2 \rangle = \frac{1}{A} \int d\rho [ \langle J_z(\boldsymbol{\rho}) J_z(\mathbf{0}) \rangle - \langle J_z \rangle^2 ], \quad (A4)$$

where  $A$  is the area of the slab surface. Correspondingly, the value of  $\langle (\delta T)^2 \rangle$  is determined by the ensemble-average fourth moment of a wave field and can be represented as an expansion in the orders of interference between ladders. Each interference event between the ladders contains the Hikami vertex [1]. The leading diagram contributing to  $\langle (\delta T)^2 \rangle$  is depicted in Fig. 2.

To calculate the Hikami vertex for nonpoint scatterers, we first consider the diagram element that describes the propagation of a wave between  $\mathbf{r}$  and  $\mathbf{r}'$  through one scatterer (see Fig. 14). This graph corresponds to the expression

$$n \int d\mathbf{r}_a \int d\mathbf{r}_1 \bar{G}(\mathbf{r} - \mathbf{r}_1) k_0^2 \varepsilon(|\mathbf{r}_1 - \mathbf{r}_a|) \bar{G}(\mathbf{r}_1 - \mathbf{r}'), \quad (A5)$$

where

$$\bar{G}(\mathbf{r} - \mathbf{r}_1) = -\frac{1}{4\pi|\mathbf{r} - \mathbf{r}_1|} \exp[(ik_0 - n\sigma/2)|\mathbf{r} - \mathbf{r}_1|] \quad (A6)$$

is the average Green's function,  $n$  is the number of scatterers per unit volume, and  $\sigma$  is the single-center scattering cross section. When integrating over the scatterer volume, we should take into account that  $|\mathbf{r}_1 - \mathbf{r}_a|$  does not exceed the scatterer size  $a$  while the characteristic scale of the Green's function decay is of the order of the mean free path  $l = (n\sigma)^{-1} \gg a$ . Therefore, it is convenient to introduce  $\mathbf{R} = \mathbf{r}_1 - \mathbf{r}_a$  and expand the Green's function arguments in powers of  $\mathbf{R}$ . If the points  $\mathbf{r}$  and  $\mathbf{r}'$  lie in the Fraunhofer zone of the scatterer ( $|\mathbf{r} - \mathbf{r}_a|, |\mathbf{r}' - \mathbf{r}_a| \gg k_0 a^2$ ),

$$|\mathbf{r} - \mathbf{r}_1| = |\mathbf{r} - \mathbf{r}_a - \mathbf{R}| \approx |\mathbf{r} - \mathbf{r}_a| - \frac{\mathbf{r} - \mathbf{r}_a}{|\mathbf{r} - \mathbf{r}_a|} \cdot \mathbf{R},$$

and transforming the Green's functions entering into Eq. (A5) as

$$\bar{G}(\mathbf{r} - \mathbf{r}_1) \approx \bar{G}(\mathbf{r} - \mathbf{r}_a) \exp(-ik_0 \boldsymbol{\Omega} \mathbf{R}), \quad (A7)$$

$$\bar{G}(\mathbf{r}_1 - \mathbf{r}') \approx \bar{G}(\mathbf{r}_a - \mathbf{r}') \exp(ik_0 \boldsymbol{\Omega}' \mathbf{R}), \quad (A8)$$

where

$$\boldsymbol{\Omega} = \frac{\mathbf{r} - \mathbf{r}_a}{|\mathbf{r} - \mathbf{r}_a|}, \quad \boldsymbol{\Omega}' = \frac{\mathbf{r}_a - \mathbf{r}'}{|\mathbf{r}_a - \mathbf{r}'|}, \quad (A9)$$

we bring Eq. (A5) to the form

$$n \int d\mathbf{r}_a \bar{G}(\mathbf{r} - \mathbf{r}_a) [-4\pi f(\boldsymbol{\Omega} \boldsymbol{\Omega}')] \bar{G}(\mathbf{r}_a - \mathbf{r}'), \quad (A10)$$

where

$$f(\boldsymbol{\Omega} \boldsymbol{\Omega}') = -\frac{1}{4\pi} \int d\mathbf{R} e^{-ik_0 \boldsymbol{\Omega} \mathbf{R}} k_0^2 \varepsilon(|\mathbf{R}|) e^{ik_0 \boldsymbol{\Omega}' \mathbf{R}} \quad (A11)$$



is the Born (or Rayleigh-Gans [47]) amplitude of scattering from  $\Omega'$  to  $\Omega$ .

Within this approximation, the equation for the ladder propagator  $\langle \psi \psi^* \rangle$  is reduced to the ordinary transport equation for the intensity  $I(\mathbf{r}, \Omega | \dots)$  in terms of which the propagator is expressed by the Wigner transform,

$$\int d\Omega \exp[ik_0\Omega(\mathbf{r} - \mathbf{r}')] I((\mathbf{r} + \mathbf{r}')/2, \Omega | \dots). \quad (\text{A12})$$

In the integral form, the transport equation for the intensity  $I(\mathbf{r}, \Omega | \dots)$  can be written as [17]:

$$\begin{aligned} I(\mathbf{r}, \Omega | \dots) &= I^{(0)}(\mathbf{r}, \Omega | \dots) + n \int d\mathbf{r}' \delta\left(\Omega - \frac{\mathbf{r} - \mathbf{r}'}{|\mathbf{r} - \mathbf{r}'|}\right) \\ &\times (4\pi)^2 |\bar{G}(\mathbf{r} - \mathbf{r}')|^2 \int d\Omega' \frac{d\sigma}{d\Omega}(\Omega\Omega') \\ &\times I(\mathbf{r}', \Omega' | \dots), \end{aligned} \quad (\text{A13})$$

where  $d\sigma(\Omega\Omega')/d\Omega = |f(\Omega\Omega')|^2$  is the differential scattering cross section, and  $I^{(0)}$  is the nonscattered intensity from a relevant source. For the incoming propagator,

$$I_i^{(0)}(z, \Omega | z_i = 0, \Omega_0) = \frac{1}{\mu_0} \delta(\Omega - \Omega_0) \exp(-n\sigma z / \mu_0), \quad (\text{A14})$$

$$\begin{aligned} &\bar{G}(\mathbf{r}_{a1} - \mathbf{r}_{a2}) \bar{G}^*(\mathbf{r}_{a2} - \mathbf{r}_{a3}) \bar{G}(\mathbf{r}_{a3} - \mathbf{r}_{a4}) \bar{G}^*(\mathbf{r}_{a4} - \mathbf{r}_{a1}) \\ &\times \exp[ik_0\Omega_{12}(\mathbf{R}'_1 - \mathbf{R}_2) - ik_0\Omega_{23}(\mathbf{R}'_2 - \mathbf{R}_3) + ik_0\Omega_{34}(\mathbf{R}'_3 - \mathbf{R}_4) - ik_0\Omega_{41}(\mathbf{R}'_4 - \mathbf{R}_1)]. \end{aligned} \quad (\text{A17})$$

The first line of Eq. (A17), which is the product of four Green's functions "connecting" the positions of four scatterers, has the same form as the empty Hikami box for a system of pointlike scatterers. The latter was calculated in Ref. [33]. The product of the Green's functions appearing in Eq. (A17) proves to be nonzero as long as the phases of the Green's functions compensate for each other. This is possible provided that the points  $\mathbf{r}_{a1}$ ,  $\mathbf{r}_{a2}$ ,  $\mathbf{r}_{a3}$ , and  $\mathbf{r}_{a4}$  lie virtually along a straight line. The alignment of these points can be found by the stationary phase method [17]. As a result, the four Green's functions entering into Eq. (A21) can be evaluated as [33]

$$\begin{aligned} &\bar{G}(\mathbf{r}_{a1} - \mathbf{r}_{a2}) \cdots \bar{G}^*(\mathbf{r}_{a4} - \mathbf{r}_{a1}) \\ &\approx (4\pi)^2 \left(\frac{2\pi}{k_0}\right)^2 \delta(\Omega_{13} - \Omega_{21}) \delta(\Omega_{13} - \Omega_{41}) \\ &\times |\bar{G}(\mathbf{r}_{a1} - \mathbf{r}_{a3})|^2 |\bar{G}(\mathbf{r}_{a2} - \mathbf{r}_{a1})|^2 |\bar{G}(\mathbf{r}_{a4} - \mathbf{r}_{a1})|^2. \end{aligned} \quad (\text{A18})$$

Expression (A18) holds for  $(\Omega_{13}\Omega_{21}) > 0$ . For  $(\Omega_{13}\Omega_{21}) < 0$ , one should substitute  $\mathbf{r}_{a3}$  for  $\mathbf{r}_{a1}$  in Eq. (A18).

The second line of Eq. (A17) contains the phase factors which, together with those in the attached ladders [see Eq. (A12)], enter into the expressions for the scattering amplitudes. When attaching the incoming and outgoing ladders to the Hikami box (A18), we take advantage of the transport equation (A13) which contains the factors appearing in Eq. (A18). As a result, the expression for the empty Hikami

$\mu_0$  is the cosine of the incidence angle. Equation (A13) stems from the Bethe-Salpeter equation for the averaged two-particle propagator to leading order in  $1/(k_0l)$  (see, e.g., Refs. [1,17]).

The diagrams for the variance  $\langle (\delta T)^2 \rangle$  can be calculated in two steps. First, we transform the product of the Green's functions entering into the Hikami vertex, and then attach the ladder propagators to it. We outline this procedure by the example of the empty Hikami box [see Fig. 2(b)].

The product of four Green's functions entering into the empty Hikami box,

$$\bar{G}(\mathbf{r}'_1 - \mathbf{r}_2) \bar{G}^*(\mathbf{r}'_2 - \mathbf{r}_3) \bar{G}(\mathbf{r}'_3 - \mathbf{r}_4) \bar{G}^*(\mathbf{r}'_4 - \mathbf{r}_1), \quad (\text{A15})$$

can be transformed with the approximate expression for the Green's function [see Eqs. (A7) and (A8)]. Using

$$\bar{G}(\mathbf{r}'_i - \mathbf{r}_k) \approx \bar{G}(\mathbf{r}_{ai} - \mathbf{r}_{ak}) \exp[ik_0\Omega_{ik}(\mathbf{R}'_i - \mathbf{R}_k)], \quad (\text{A16})$$

where  $\mathbf{R}'_i = \mathbf{r}'_i - \mathbf{r}_{ai}$ ,  $\mathbf{R}_k = \mathbf{r}_k - \mathbf{r}_{ak}$ , and  $\Omega_{ik} = (\mathbf{r}_{ai} - \mathbf{r}_{ak})/|\mathbf{r}_{ai} - \mathbf{r}_{ak}|$ , we represent Eq. (A15) in the form

box with attached ladders takes the form

$$\begin{aligned} \langle (\delta T)^2 \rangle &= \frac{\pi}{N} n \int_0^L dz \iint d\Omega d\Omega' \frac{d\sigma}{d\Omega}(\Omega\Omega') \\ &\times [I_f^2(L|z, \Omega) I_i^{\text{sc}}(z, \Omega) I_i(z, \Omega') \\ &+ I_f^2(L|z, \Omega') I_i(z, \Omega) I_i^{\text{sc}}(z, \Omega')], \end{aligned} \quad (\text{A19})$$

where the scattered intensity is defined as  $I^{\text{sc}} = I - I^{(0)}$ . Equation (A19) should be supplemented by the contribution from the diagrams containing incoming propagators with no scattering events. The calculation of these diagrams gives the expression that differs from Eq. (A19) by substitution of  $I^{(0)}$  for  $I^{\text{sc}}$ . Thus, the final expression for the empty-Hikami-box contribution to the variance  $\langle (\delta T)^2 \rangle$  differs from Eq. (A19) only by omitting the superscript "sc" in the incoming propagators.

In a similar way, the contribution from the other two diagrams involving the Hikami box with one extra scattering [see Fig. 2(b)] can be calculated. Using the representation for the Green's functions (A16) and repeating the corresponding calculations performed for pointlike scatterers in Ref. [33], we arrive at the expressions that differ from those for pointlike scatterers only by the presence of the angle-dependent differential cross section. Combining the contributions to the variance  $\langle (\delta T)^2 \rangle$  from each diagram shown in Fig. 2(b) we obtain Eq. (3).

## APPENDIX B: CONDITIONS FOR NEGLECTING THE COHERENT REFLECTION FROM THE BOUNDARIES

Under the conditions of refractive-index matching (see, e.g., Refs. [41–43]), the average refractive index of the disordered sample is due to only the scattering particles. Its relative value  $\langle m \rangle$  is expressed in terms of the amplitude of scattering through the zero angle  $f(0)$  as follows [17],

$$\langle m \rangle = 1 + \frac{2\pi n f(0)}{k_0^2}, \quad (\text{B1})$$

where  $n$  is the number of scatterers per unit volume,  $k_0 = 2\pi/\lambda$  is the wave number, and  $\lambda$  is the wavelength of light in the surrounding uniform medium. The effect of coherent reflection on wave transport in the sample at oblique incidence (up to grazing angles) can be neglected provided that  $\sqrt{|\langle m \rangle - 1|}$  is less than the characteristic single-scattering angle  $\vartheta_0 \sim \lambda/a$  ( $a$  is the particle size). From this condition and Eq. (B1) it follows that, for weak scatterers  $[k_0 a |m - 1| \ll 1$ ,  $m$  is the refractive index of the particles,  $\text{Re } f(0) \gg \text{Im } f(0)$  [47]], the inequality

$$n a^3 |m - 1| \ll \vartheta_0^2 \quad (\text{B2})$$

should be fulfilled. For strong scatterers  $[k_0 a |m - 1| > 1$ ,  $\text{Re } f(0) \ll \text{Im } f(0)$  [47]], we arrive at the restriction

$$\frac{1}{k_0 l} \ll \vartheta_0^2, \quad (\text{B3})$$

where the mean free path  $l$  is expressed in terms of  $n$  and  $f(0)$  via the optical theorem. The latter inequality can be rewritten as

$$k_0 a^2 \ll l, \quad (\text{B4})$$

and it means that successive scattering events occur in the Fraunhofer zone of an individual scattering particle. Under condition (B2), this is certainly satisfied as well.

As was shown in Ref. [48], only under condition (B4), transmission fluctuations are described by the single-Hikami-vertex diagram depicted in Fig. 2. Otherwise ( $k_0 a^2 \gg l$ ), this diagram should be replaced by another one. Such a case is specific to a continuous random medium with extremely large inhomogeneities (e.g., turbulent atmosphere) [17,49,50].

- 
- [1] E. Akkermans and G. Montambaux, *Mesoscopic Physics of Electrons and Photons* (Cambridge University Press, Cambridge, UK, 2011).
- [2] S. M. Popoff, A. Goetschy, S. F. Liew, A. D. Stone, and H. Cao, *Phys. Rev. Lett.* **112**, 133903 (2014).
- [3] O. S. Ojambati, J. T. Hosmer-Quint, K.-J. Gorter, A. P. Mosk, and W. L. Vos, *Phys. Rev. A* **94**, 043834 (2016).
- [4] C. W. Hsu, S. F. Liew, A. Goetschy, H. Cao, and A. D. Stone, *Nat. Phys.* **13**, 497 (2017).
- [5] S. Rotter and S. Gigan, *Rev. Mod. Phys.* **89**, 015005 (2017).
- [6] J. Bertolotti, E. G. van Putten, C. Blum, A. Lagendijk, W. L. Vos, and A. P. Mosk, *Nature (London)* **491**, 232 (2012).
- [7] O. Katz, P. Heidmann, M. Fink, and S. Gigan, *Nat. Photonics* **8**, 784 (2014).
- [8] R. Carminati, G. Cwilich, L. S. Froufe-Perez, and J. J. Saenz, *Phys. Rev. A* **91**, 023807 (2015).
- [9] N. Fayard, A. Caze, R. Pierrat, and R. Carminati, *Phys. Rev. A* **92**, 033827 (2015).
- [10] B. Judkewitz, R. Horstmeyer, I. M. Vellekoop, I. N. Papadopoulos, and C. Yang, *Nat. Phys.* **11**, 684 (2015).
- [11] G. Osnabrugge, R. Horstmeyer, I. N. Papadopoulos, B. Judkewitz, and I. M. Vellekoop, *Optica* **4**, 886 (2017).
- [12] T. J. Arruda, A. S. Martinez, and F. A. Pinheiro, *Phys. Rev. A* **98**, 043855 (2018).
- [13] A. M. Paniagua-Diaz, I. Starshynov, N. Fayard, A. Goetschy, R. Pierrat, R. Carminati, and J. Bertolotti, *Optica* **6**, 460 (2019).
- [14] N. Fayard, A. Goetschy, R. Pierrat, and R. Carminati, *Phys. Rev. Lett.* **120**, 073901 (2018).
- [15] I. Starshynov, A. M. Paniagua-Diaz, N. Fayard, A. Goetschy, R. Pierrat, R. Carminati, and J. Bertolotti, *Phys. Rev. X* **8**, 021041 (2018).
- [16] M. C. W. van Rossum and Th. M. Nieuwenhuizen, *Rev. Mod. Phys.* **71**, 313 (1999).
- [17] A. Ishimaru, *Wave Propagation and Scattering in Random Media* (Wiley-IEEE, New York, 1997).
- [18] O. B. Firsov, *Sov. Phys. Dokl.* **11**, 732 (1967).
- [19] O. B. Firsov, E. S. Mashkova, V. A. Molchanov, and V. A. Snisar, *Nucl. Instrum. Methods* **132**, 695 (1976).
- [20] V. S. Remizovich, M. I. Ryazanov, and I. S. Tilinin, *Sov. Phys. JETP* **52**, 225 (1980).
- [21] V. S. Remizovich, M. I. Ryazanov, and I. S. Tilinin, *Sov. Phys. Dokl.* **25**, 751 (1980).
- [22] A. I. Kuzovlev and V. S. Remizovich, *Phys. Rev. A* **48**, 465 (1993).
- [23] V. S. Remizovich, *Sov. Phys. JETP* **60**, 290 (1984).
- [24] A. I. Kuzovlev and V. S. Remizovich, *Laser Phys.* **2**, 262 (1992).
- [25] C. W. J. Beenakker, *Rev. Mod. Phys.* **69**, 731 (1997).
- [26] L. I. Glazman and M. Jonson, *Phys. Rev. B* **44**, 3810 (1991).
- [27] V. V. Marinyuk and D. B. Rogozkin, *Phys. Rev. B* **91**, 125125 (2015).
- [28] S. Hikami, *Phys. Rev. B* **24**, 2671 (1981).
- [29] M. J. Stephen and G. Cwilich, *Phys. Rev. Lett.* **59**, 285 (1987).
- [30] S. Feng, C. Kane, P. A. Lee, and A. D. Stone, *Phys. Rev. Lett.* **61**, 834 (1988).
- [31] E. Akkermans and G. Montambaux, *J. Opt. Soc. Am. B* **21**, 101 (2004).
- [32] D. B. Rogozkin and M. Yu. Cherkasov, *JETP Lett.* **58**, 585 (1993).
- [33] D. B. Rogozkin and M. Yu. Cherkasov, *Phys. Rev. B* **51**, 12256 (1995).
- [34] D. B. Rogozkin, *JETP* **84**, 916 (1997).
- [35] O. Agam, A. V. Andreev, and B. Spivak, *Phys. Rev. Lett.* **97**, 223901 (2006).
- [36] O. Agam, A. V. Andreev, and B. Spivak, *Phys. Rev. B* **76**, 174204 (2007).

- [37] H. C. van de Hulst, *Multiple Light Scattering: Tables, Formulas, and Applications*, Vols. 1 and 2 (Academic, New York, 1980).
- [38] K. Vynck, R. Pierrat, and R. Carminati, *Phys. Rev. A* **94**, 033851 (2016).
- [39] K. Stamnes, S. C. Tsay, W. Wiscombe, and K. Jayaweera, *Appl. Opt.* **27**, 2502 (1988).
- [40] V. V. Marinyuk and S. V. Sheberstov, *Opt. Lett.* **41**, 922 (2016).
- [41] R. N. Wolfe, J. J. DePalma, and S. B. Saunders, *J. Opt. Soc. Am.* **55**, 956 (1965).
- [42] D. S. Wiersma, M. P. van Albada, B. A. van Tiggelen, and A. Lagendijk, *Phys. Rev. Lett.* **74**, 4193 (1995).
- [43] A. Stipp, H.-J. Schöpe, Th. Palberg, Th. Eckert, R. Biehl, and E. Bartsch, *Phys. Rev. E* **81**, 051401 (2010).
- [44] M. Gao, X. Huang, P. Yang, and G. W. Kattawar, *Appl. Opt.* **52**, 5869 (2013).
- [45] A. Garcia-Martin, F. Scheffold, M. Nieto-Vesperinas, and J. J. Saenz, *Phys. Rev. Lett.* **88**, 143901 (2002).
- [46] L. S. Froufe-Perez, A. Garcia-Martin, G. Cwilich, and J. J. Saenz, *Physica A* **386**, 625 (2007).
- [47] H. C. van de Hulst, *Light Scattering by Small Particles* (Dover, New York, 1981).
- [48] D. B. Rogozkin and M. Yu. Cherkasov, *Phys. Lett. A* **178**, 431 (1993).
- [49] A. M. Prokhorov, F. V. Bunkin, K. S. Gochelashvily, and V. I. Shishov, *Proc. IEEE* **63**, 790 (1975).
- [50] J. L. Codona, D. B. Creamer, S. M. Flatte, R. G. Frehlich, and F. S. Henyey, *Radio Sci.* **21**, 929 (1986).